FUDMA Journal of Engineering and Technology
ISSN: 3092-9385
https://sites.google.com/fudutsinma.edu.ng/fjet
Volume 1, Issue 2, 2025, 425-435

Optical and Structural Properties of Er/Sr Co-Doped αMnS Films Prepared by Chemical Spray Pyrolysis

Onyeka E. NNANYELUGO[1*], Peter O. OFFOR[2], Cyril OCHERI[3], Camillus S. OBAYI[4]

[1*,2,3,4]Department of Metallurgical and Materials Engineering, University of Nigeria, Nsukka, Nigeria

[1*]onyeka.nnanyelugo@unn.edu.ng, [2]peter.offor@unn.edu.ng, [3]cyril.ocheri@unn.edu.ng, [4]camilius.obayi@unn.edu.ng

Abstract

Erbium/Srontium (Er/Sr) co-doped α manganese sulphide (αMnS) thin films were synthesized via chemical spray pyrolysis and characterized using UV-Vis, SEM/EDS, FTIR, and XRD. Optimal optical properties were observed at 10ml Er/Sr doping, with a reduced bandgap of 2.33 eV and improved absorbance. SEM revealed enhanced grain connectivity, while XRD confirmed the retention of cubic structure. These results suggest potential applications in optoelectronics. These films were made from a precursor solution containing 0.8451M manganese (II) sulphate ($MnSO_4.H_2O$), 0.1M thioacetamide (CH_3CSNH_2), 0.85M strontium hydroxide ($Sr(OH)_2$), and 0.95M Erbium (III) chloride hexahydrate ($ErCl_3.6H_2O$), which were spray-coated on a glass substrate at constant temperature of 300°C. The samples were characterized using different techniques such as scanning electron microscope (SEM)/EDS, UV-Visible spectroscopy, Fourier transform infrared (FTIR), and X-ray diffraction (XRD) analysis. The SEM and EDS analysis revealed that moderate doping (≤10%) enhances grain connectivity and crystal growth in the sample, resulting in a more compact structure with improved crystallinity. The EDS indicate the elements in wt.% (%), the elemental composition such as Mn, S, Er, and Sr. The UV-Visible spectroscopy study revealed an improved optical property for all the samples, but it's more prominent in the sample synthesized with 10ml Er/Sr. The FTIR result showed that some functional groups like C=O, C–H, N–H, S-O, αMn-S, and O-H were present. As revealed by XRD analysis revealed the physical interpretation of the crystal planes (111), (220), (200), (311), and (222), respectively.

Keywords: *Erbium/strontium, doped, thin film, chemical, spray pyrolysis.*

1.0 Introduction

Due to their numerous uses and distinct electronic, optical, and magnetic characteristics, nanocrystalline films are beneficial to many electrical and optical sectors today [1]. As a result, dilute magnetic semiconducting (DMS) thin films are the focus of intense research effort and have shown promise in applications [2]. Dilute magnetic semiconductors include manganese sulphide (MnS). Shrinking manganese sulphide (MnS) into the nanometric zone (1-100 nm) changes its bulk properties, making it a material of interest for basic and applied research [3]. Numerous applications, such as optoelectronics, photovoltaics, sensors, and spintronics, have demonstrated potential for MnS thin films [4]. Manganese sulphide is a semiconductor related to the p-type group VII-VI, with a broad band-gap between 2.7 and 3.7 eV. It has three distinct crystalline phases: α-MnS, which has a stable rock-salt structure; β-MnS, which has a metastable zinc blende structure; and γ-MnS, which has a wurtzite structure [5][6]. A wide bandgap has been said to be beneficial in MnS since it gives this semiconductor special characteristics that make it a strong contender for UV emission [7]. Wide band gap semiconductors' high resistivity, however, restricts how much energy they can absorb from the visible portion of the solar spectrum [8][9]. Doping is the only method to address poor absorption of energy from specific sun spectrum regions. In contrast to pristine nanostructures, doped nanostructures have distinct chemical and physical characteristics because they generate distinct energy levels within the inherent quantum energy levels, improving the host semiconductor's electrical, magnetic, and optical characteristics [10]. Lead [11], mercury [12], and zinc [13] have all been used to adjust manganese sulphide in the past. According to Bulakhe[11], his research on Pb-doped MnS thin films resulted in a film with better optical qualities and a lower energy bandgap. Doping MnS changes its magnetic characteristics in addition to its enhanced optical characteristics [14]. Reports of doping manganese sulphide with two or more elements are scarce, nevertheless.

Co-doping has several benefits since the combination of ions affects characteristics that a single ion could not provide, which may make the film suitable for use in a variety of fields. Research indicates that temperature, particle size, precursor solution concentration, and synthesis technique all affect the characteristics of doped and undoped MnS thin films [15]. MnS thin films have been produced using a variety of techniques, including spray pyrolysis [18], electrodeposition [17], chemical bath deposition [16], and solvothermal synthesis [5]. Sadly, a number of these methods have some shortcomings, such as weak crystallization, poor adhesion, uneven films, or the amorphous form of some films, which necessitate a post-annealing treatment in the case of chemical bath deposition in order to attain sufficient crystallinity [19]. Spray pyrolysis has been demonstrated to be the most

Received: 10/07/2025; Revised: 21/07/2025; Accepted: 29/07/2025; Published: 15/09/2025

effective of these methods due to its ease of use, low cost, and ability to deposit smooth, homogenous, and uniform layers [20–21]

Over the past ten years, manganese sulphide has been one of the materials most thoroughly studied in an attempt to improve the electrical, optical, and magnetic characteristics of nanostructured semiconductors [22–24]. Manganese-containing materials are intriguing due to their extensive use in numerous fields of contemporary technology, exceptional magneto-optical characteristics, and intriguing magnetism and semi conductivity combination [17]. The most common polymorphs of manganese sulphide are MnS2 (cubic), β-MnS (zinc blende), γ-MnS (wurtzite), and α-MnS (rock salt) [25]. The most prevalent form among all rock types is the salt type [26].

MnS thin film deposition Because manganese sulphide particles are employed in both optoelectronics and optical systems, the methods used to synthesis them are crucial [27]. According to Adam & Ramamurthi [28], the thickness, size, and production process all have an equal impact on the qualities of the deposited thin film in addition to the thin film's form. Nonetheless, a variety of techniques, including sol-gel synthesis [29], hydrothermal conditions [30], chemical vapour deposition [31], microwave irradiation and ultrasonic spray approach [32], and spray pyrolysis [33], could be used to create manganese sulphide. The study's goal is to examine the optical and structural characteristics of er/sr co-doped mns films prepared by chemical spray pyrolysis. Al-Diabat et al., [34] reaffirmed that selecting a thin film deposition technique has several factors to take into account, including the cost, the simplicity of fabrication, and the suitability that the material can fabricate.

The most popular method for thin film deposition is chemical spray pyrolysis because of its ease of application, affordable price, and ability to produce smooth, homogenous, and uniform layers. [35]. According to Ajayi et al. [36], the spray pyrolysis process is unique among approaches due to its industrial scalability, versatility, and easy controllability of stoichiometry. Almost any element can be deposited using the spray pyrolysis process [20]. According to Falcony et al. [37], the chemical spray pyrolysis process is a way to create a material using chemicals at atmospheric pressure. This method creates the thin films or powders by pressure spraying a precursor solution made from a chemical compound that has been dissolved in the necessary solvent onto a heated glass substrate. However, ultrasonic and pneumatic systems are typically employed to generate the aerosol used for the spraying operation, and the settings are typically optimized to yield the necessary qualities. A precursor solution, an atomizer, an ambient temperature controller, and a substrate heater make up a typical spray pyrolysis setup [38].

2.0 Materials and Methods

2.1 Materials

The required chemicals (Erbium chloride ($ErCl_3$), strontium chloride ($SrCl_2$), manganese chloride ($MnCl_3$), and thioacetamide (CH_3CSNH_2)) and glass substrate (florine doped tin oxide) were gotten from Jeochem chemical store, opposite bishop shanahan hospital Nsukka.

2.2 Equipment

The experimental study was carried out at the physics nano-laboratory, University of Nigeria, Nsukka. Ultra sonication device, beaker, magnetic stirrer, digital weighing balance, spatula, drying oven, spray pyrolysis machine, soda-lime glass, scanning electron microscope (SEM), X-ray diffraction (XRD), Energy Dispersive Spectroscopy (EDS), UV-Visible Spectrophotometry and photoluminescence (PL) spectroscopy are the equipment employed to study the deposited thin films.

2.3 Methods

2.3.1 Preparation of the substrate

The glass substrates of dimensions 30mm × 25mm × 1.2 mm were washed with soap and distilled water first, then submerged for 10 minutes in acetone, and rinsed with distilled water twice after being withdrawn from the acetone. It was transferred to another beaker containing distilled water and then put through an ultrasonic bath containing distilled water for 15 minutes. After that, the substrates were withdrawn from the ultasonicator, followed by drying in an oven, making sure that dirt is avoided. Because according to the study released by Sarki et al., [39], thorough cleaning was necessary since the degree of the thin film's adherence depends on the purity of the substrate.

2.3.2 Precursor solution formulation

For this experiment, analytical-grade chemicals were used. They include Erbium (III) chloride hexahydrate, Strontium hydroxide, manganese (II) sulphate and thioacetamide. These listed chemicals served as the sources of Er, Sr, Mn, and S ions respectively. Before the preparation of the precursor solution, a molarity calculation for each reagent was done and was obtained as 0.8451M manganese (II) sulphate $MnSO_4.H_2O$, 0.1M thioacetamide CH_3CSNH_2, 0.85M strontium hydroxide Sr $(OH)_2$ and 0.95M Erbium (III) chloride hexahydrate $ErCl_3.6H_2O$. After the calculation, the individual solutions were prepared separately using distilled water as solvent. Followed by stirring using a magnetic stirrer for about 10hr [18]. Finally, the prepared solutions were covered in a beaker

Received: 10/07/2025; Revised: 21/07/2025; Accepted: 29/07/2025; Published: 15/09/2025

and allowed to stay for 24hrs to make sure that the particle dissolved completely. For the final volume of the precursor that was sprayed, the required volume of each solution in ml were measured out, mixed and was used for spray coating. Table 1 and 2 show the detailed information of the chemicals used and the formulated precursor solution sprayed at contant temperature of 300^{o}C used for the coating.

Table 1: Chemicals used and their details

Reagent Name	**Chemical Formulae**	**Molecular Weight (g/mol)**
Erbium (III) Chloride Hexahydrate	$ErCl_3.6H_2O$	381.71
Strontium Hydroxide	$Sr(OH)_2$	121.63
manganese (II) sulphate	$MnSO_4.H_2O$	151
Thioacetamide	CH_3CSNH_2	75.13
Acetone	CH_3COOCH_3	58.08

Table.2: Formulated precursor solution sprayed at constant temperature of 300°C

S/N	**Manganese (II) Sulphate ($MnSO_4.H_2O$)**	**Thioacetamide (CH_3CSNH_2)**	**Strontium Hydroxide ($Sr(OH)_2$)**	**Erbium (III) Chloride Hexahydrate ($ErCl_3.6H_2O$)**	**Final Volume**
1	10 ml	10 ml	0 ml	0 ml	20 ml
2	10 ml	10 ml	5 ml	5 ml	30 ml
3	10 ml	10 ml	10 ml	10 ml	40 ml
4	10 ml	10 ml	15 ml	15 ml	50 ml
5	10 ml	10 ml	20 ml	20 ml	60 ml

2.3.3 Thin film production

When the spray pyrolysis machine was turned on, we set the temperature to be 300°C. The substrate was then placed on the heater and allowed to be heated to the same temperature of 300°C before pouring the formulated precursor solution into a collecting funnel. The solution flowed through the nozzle and pressure sprayed on the glass substrate. The spray rate, pressure, and distance separating the nozzle and heated substrate were 4kg/cm^2 25–50 kg/cm^2, and 20kg/cm^2 respectively. The same process was repeated until the required number of films was achieved.

2.5 Characterization

The Er/Sr doped and undoped MnS thin films synthesized were characterized using the;

i. UV-Visible Spectrophotometry for optical properties of the deposited thin films.
ii. Scanning electron microscope (SEM) and EDX to examine the morphology and the possible elemental constituents.
iii. X-ray diffraction (XRD) to investigate the structural properties and phases present.
iv. Fourier transform infrared spectroscopy (FTIR) to determine the functional groups contained in the films.

3.0 Results and Discussion

3.1 UV-Visible Study

To examine the optical properties of the synthesized thin films, UV-Visible spectroscopy which is non-destructive, simple, cost-effective analytic technique was used, it measures the transmittance or absorbance of incident ray passing through a substance [40]. The data obtained from absorbance equally gave information on the refractive index, optical conductivity, reflectance and energy bandgap. This study was conducted at the range of wavelength of 400nm-1100nm.

3.2 Absorbance

Figure 1 presents the absorbance of the samples in UV-Visible region. A simple equation founded by **[**81] was used to calculate the absorbance of the samples. The equation is given as

$$\alpha = 2.303A/1 \qquad (1)$$

α, l and A are the parameters representing coefficient of absorption, path length and absorbance respectively. Figure 1 shows the absorbance of the doped thin film with 10Er,10Sr has the highest absorbance peak of 0.5 au followed by the one containing 5Er,5Sr having peak at 0.27 a.u. The sample with the lowest absorption peak was the ZnS pristine. All the samples have their noticeable peaks within the visible region of the spectra, which is an

Received: 10/07/2025; Revised: 21/07/2025; Accepted: 29/07/2025; Published: 15/09/2025

indication that they are good candidate for solar cell application. The results we obtained are in agreement with the report published by [41] However, there is a slight discrepancy between our findings and the result published by [42] which reported that the thin film they synthesized with 5ml (Bi, Sr) has the highest absorption peak in the visible region. Similar to the result obtained in literature [43], our graph shows that all the samples possess only one peak, and the position of each peak differ from one another as the volume concentration of the impurity ion occupying the lattice points of MnS changes.

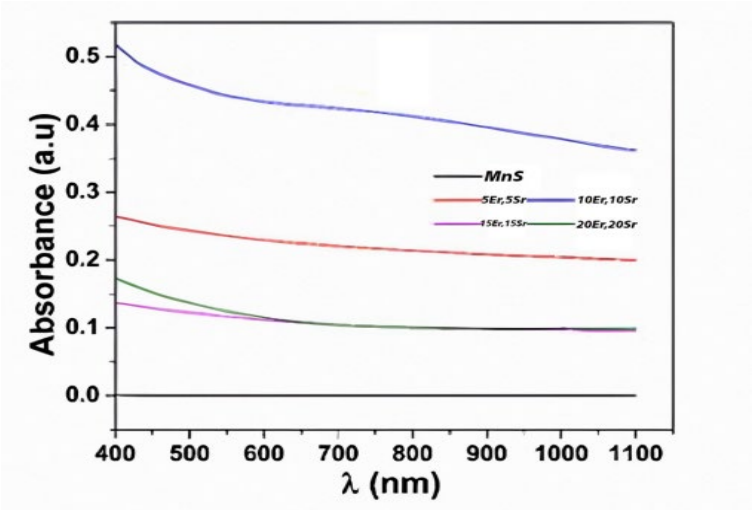

Figure 1: Absorbance of the samples in UV-Visible region

3.3 Transmittance

Figure 2 is the graph of the transmittance of the samples, examined in the wavelength range of 400nm to 1100nm. The graph revealed that the transmittance of the samples MnS, 5ml (Er, Sr), 10ml (Er, Sr), 15ml (Er, Sr) and 20ml (Er, Sr) are 100%, 54%, 35%, 75% and 75% respectively. However, it was observed that the transmittance of the pure MnS is higher within the visible region than the doped samples which have low percentage transmittance between 35%-75%. Moreover, among the doped samples, the film doped with 10ml (Er, Sr) has the least percentage of transmittance. The changes in the transmittance percentages of the doped MnS is as the result of thin film thickness variation, this result follows the same trend with finding reported by [24]. Additionally, increased percentage transmittance values for the doped samples could as well be caused by grain concentration which brought about the roughness increment on the surfaces of the samples leading to transmittance reduction [44].

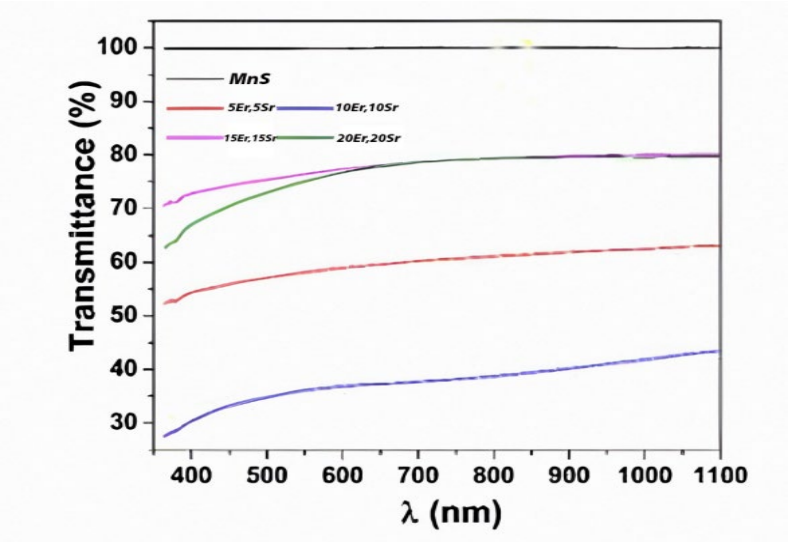

Figure 2: Transmittance measurement (400nm to 1100nm.)

3.4 Reflectance

Figure 3 is the graph showing the reflectance of the obtained thin films. The optical reflectance spectra of the thin films were carried out within the wavelength range of 400nm-1100nm and the reflectance was also calculated using the expression in equation 2 below,

Received: 10/07/2025; Revised: 21/07/2025; Accepted: 29/07/2025; Published: 15/09/2025

$$R = 1 - T - A \quad (2)$$

where A represents the absorbance, T is the transmittance and reflectance R [33], Figure 3 within the visible region, the thin film synthesized with 10ml (Er, Sr) impurities showed highest peak of reflectance 72%, followed by the sample containing 5ml (Er, Sr) dopants with the peak value of 47%. The samples with 15ml (Er, Sr) and 20ml (Er, Sr) of impurities have percentage reflectance of 30% and 35% respectively. However, within the wavelength of 600nm-1100nm, the reflectance of both samples merged together and decreased simultaneously along the spectra. We also observed that the control has the lowest reflectance of 0%. Generally, the graph showed that as the wavelength of the solar spectra increases, the reflectance of all the samples decreases except the control. Result with similar nature was published by [24]

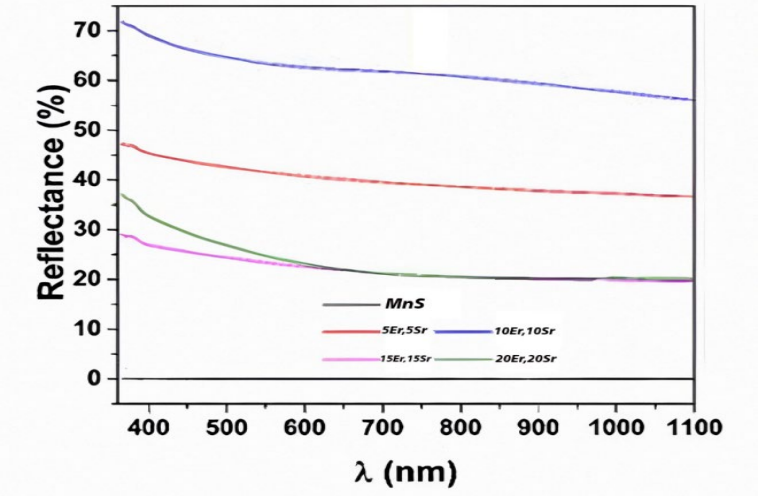

Figure 3: Optical rreflectance of the spectra

3.5 Bandgap energy

Figure 4 is a graph showing the energy bandgap of the thin films spray coated with pure MnS, 5ml (Er, Sr), 10ml (Er, Sr), 15ml (Er, Sr) and 20ml (Er, Sr). The energy bandgap of each sample was determine using a formula formulated by [45],

$$(\alpha h\nu)^{\frac{1}{n}} = A(h\nu - Eg) \quad (3)$$

where Eg, hv, α and A represents energy bandgap, photon energy, coefficient of absorption and constant respectively, whereas n stands for direct or indirect transition. If $(\alpha h\nu)^2$ is equated to zero when the linear portion of the graph is extrapolated, we observed that the energy bandgaps of all the synthesized thin films are 3.33eV, 2.77 eV, 2.33 eV, 3.18 eV and 3.28 eV respectively. In comparison with pure MnS, all the doped MnS thin films have decreased energy bandgap. This finding is in resonance with the result published by [23]. The decrease in the energy bandgap of the doped samples could be as a result of the effect of near band levels [43].

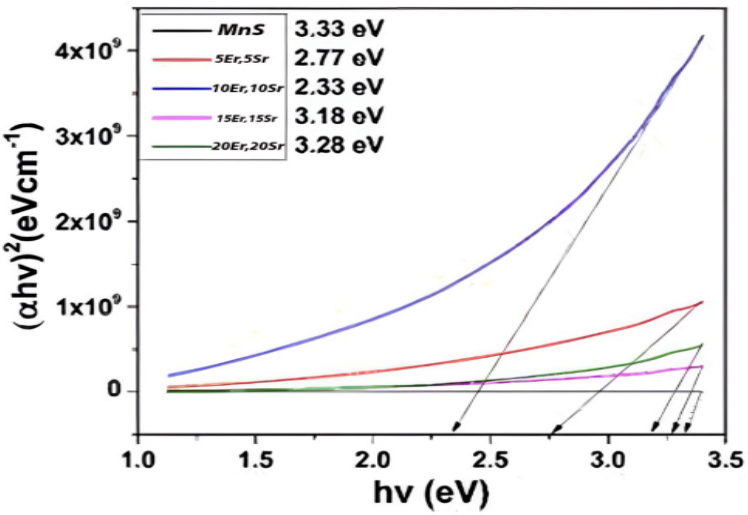

Figure 4: Energy bandgap of the thin films spray coated with pure MnS

Received: 10/07/2025; Revised: 21/07/2025; Accepted: 29/07/2025; Published: 15/09/2025

3.6 SEM and EDS Studies

Figure 5 and 6 are the SEM/EDS images of the sample thin films MnS, 5ml (Er,Sr), MnS, 10ml (Er,Sr), MnS, 15ml (Er,Sr), MnS, and 20ml (Er,Sr), MnS. From the figure, the surface morphology of the sample MnS revealed less granular structure, with fine grain size showing minimal nucleation growth. The sample is homogenous and has low porosity indicating that the matrix of the MnS was not altered. The SEM demonstrated that the surface morphology of sample 5ml (Er, Sr), MnS was considerably more uneven than the control, as shown by the small collections in the morphology.

This sample has slightly increased grain size with a better-defined grain boundary when compared with the pristine. The incorporation of small amount of Er/Sr into the matrix of the pristine may have likely improved nucleation sites of the MnS promoting crystal growth. Sample 10ml (Er,Sr),MnS has similar nature with sample 5ml (Er,Sr),MnS. However, it has more significantly increased grain size and the particles were uniformly distributed but with minimal clusters. This sample is more compacted when compared to others, which could likely caused by improved film quality. Result from this particular sample indicates that moderate doping enhances grain connectivity and crystal growth. The concentration of Er/Sr dopants used in synthesizing this sample fall within the optimal range ≤10% as reported in other scholarly works. This could be the reason this sample gave a better crystallinity with reduced defects. Sample 15ml (Er,Sr),MnS revealed dense film that possess bigger grain structures, indicating coalescence. Sample 20ml (Er,Sr),MnS looks more dense and has cracks, indicating over doping, which resulted to more porosity when compared with other samples. The grain sizes are irregular due to over doping distorting the crystal growth pattern. It has been reported that excessive doping leads to the segregation of secondary phase or defects induced by strain [46]. The EDS analysis revealed the elemental composition of the deposited thin films. Figures 7 and 8 show the SEM/ EDS of 5ml (Er, Sr) Mns, Figures 9 and 10 indicate the SEM/EDS of 10ml (Er, Sr) mns , Figures 11 and 12 depict SEM/EDS of 15ml (Er, Sr) mns, Figures 13and 14 show the SEM/ EDS of 20ml (Er, Sr) mns The SEM morphology shows improvement in the addition of the varied concentration through the process. The EDS revealed the element in wt(%) indicating the elements that are present such are such as Mn, Er, Sr and S. However, the presence of other elements like Si, Ca, Na and Mg were noticed in the EDS results indicating that there were pick up of such elements from either the glass substrate, atmosphere or scanning electron microscope chamber effect [47].

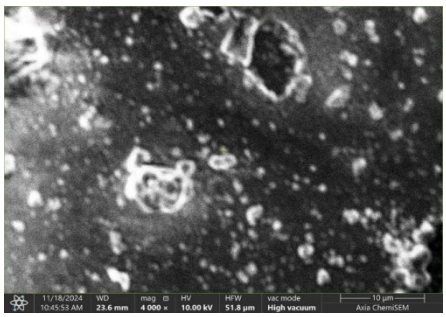

Figure 5 SEM Mns

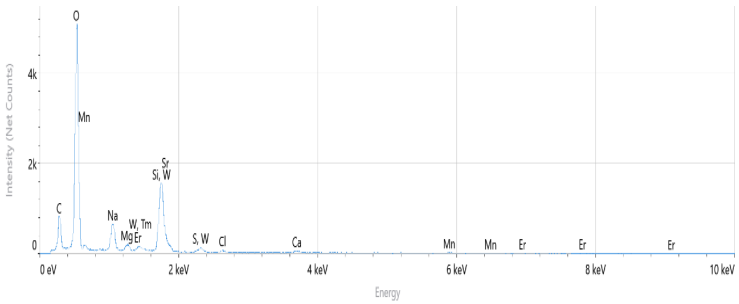

Figure 6 EDS Mns

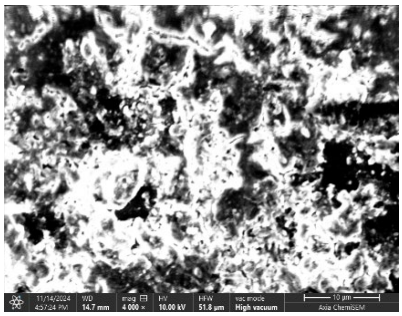

Figure 7 SEM 5ml (Er, Sr) Mns

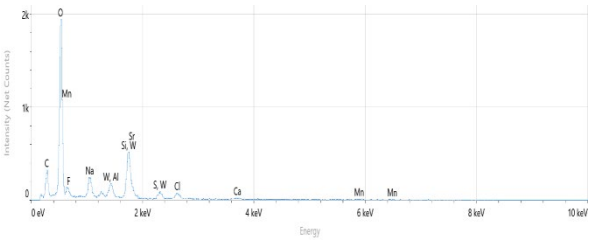

Figure 8 EDS 5ml (Er, Sr) mns

Received: 10/07/2025; Revised: 21/07/2025; Accepted: 29/07/2025; Published: 15/09/2025

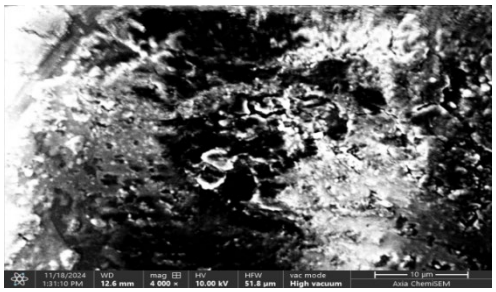

Figure 9 SEM 10ml (Er, Sr) mns

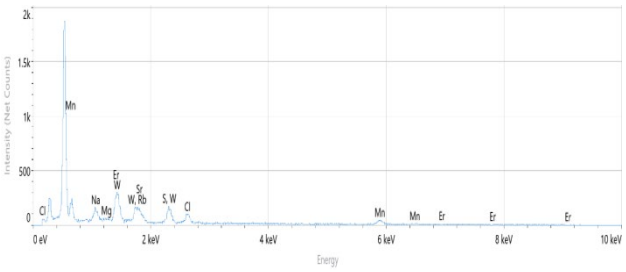

Figure 10 EDS 10ml (Er, Sr) mns

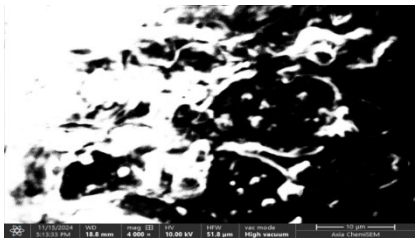

Figure 11 SEM 15ml (Er, Sr) mns

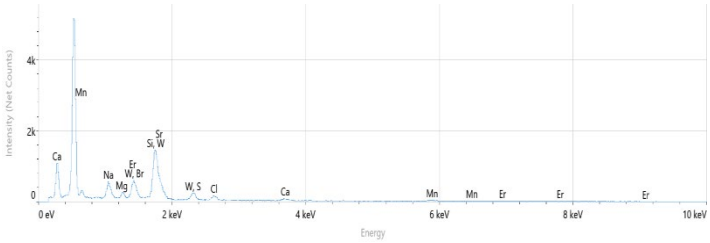

Figure 12 EDS 15ml (Er, Sr) mns

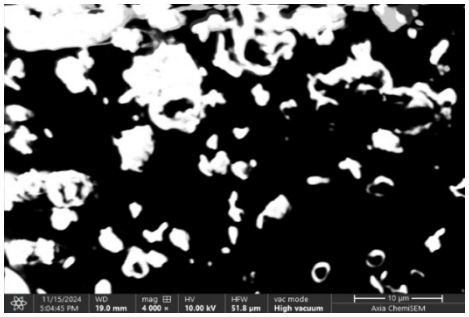

Figure 13 SEM 20ml (Er, Sr) mns

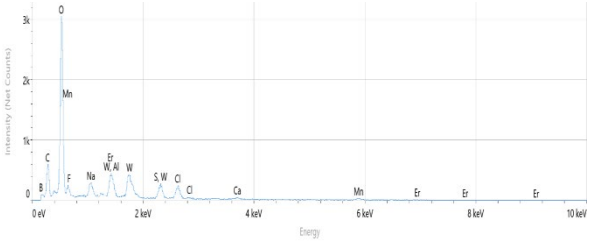

Figure 14 EDS 20ml (Er, Sr) mns

3.7 Fourier Transform Infrared (FTIR) Analysis

Figure11 is the Fourier transform infrared (FTIR) graph of the synthesized thin films. The study was carried out within the wavelength range of 500-4000cm^{-1}. From the figure, it was observed that in the wavelength region of 500–700 cm^{-1} stretching vibration of Mn-S fully occur in all the samples. However, the characteristic peaks were more prominent in the samples MnS and 15ml (Er,Sr), MnS showing higher transmittance. The broader peaks noticed could mean lattice distortion due to incorporated impurities [48]. However, there was a shift in the positions of Mn-S band and width as the concentration of the impurities increase, showing lattice perturbation by these impurities Er/Sr, a trend which is in agreement with previous doping experiments [48].

Region 900–1200 cm^{1} indicates a stronger peak, and it's more noticeable in samples 10ml (Er, Sr), MnS, 5ml (Er, Sr), MnS, and 20ml (Er, Sr): MnS, showing a decrease in transmittance, indicating an increase in absorption. S-O vibration occurs within this region, and it is believed to have originated from sulphure oxidation during synthesis. It has been reported that increased intensity in thin films could be because of high thickness of the film or higher interaction between the glass substrate and film or oxidation at the surface of the film [49], [50].

Between 1300–3000 cm^{1}region occurs weak peaks. These peaks may have come from stretching or bending of C=O, C, H or N–H functional groups originating from the precursor solution. Liao et al. reported that when semiconductors from group II–VI are doped, the occurring functional group usually comes from the precursor solution [51] Region 3200–3600 cm^{1} shows a very weak band in all the samples and corresponds to the stretching vibration of O-H. This functional group is suspected to have come from adsorbed water or hydroxyl groups in the film, suggesting incomplete dehydration. However, in samples with high concentrations of dopants, broader O–H bands were observed, which could be a result of more defect sites in the films. Similar to other works of

Received: 10/07/2025; Revised: 21/07/2025; Accepted: 29/07/2025; Published: 15/09/2025

literature, hydroxylation has been reported to increase with increase in film disorder or increase in dopant concentration [51].

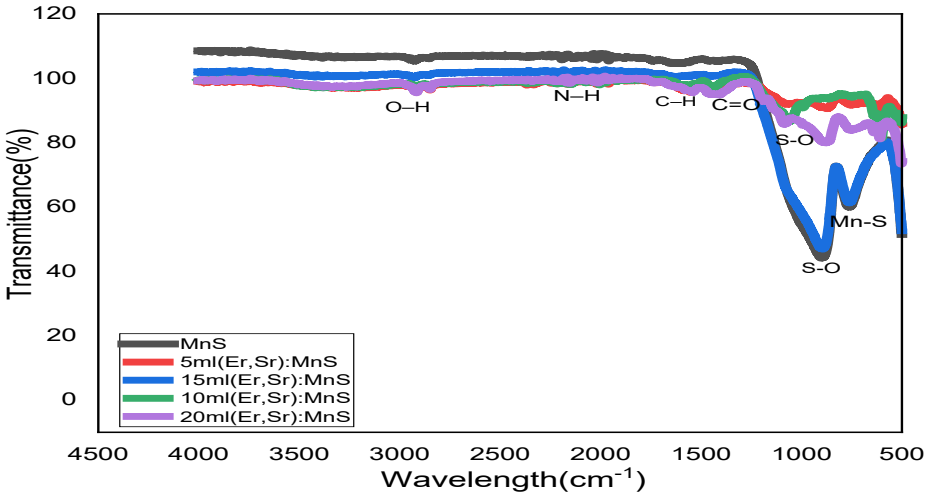

Figure 11: FTIR of the doped samples

3.8 X-ray Diffraction (XRD) Analysis

Figure 12 is the graph of the XRD of the samples. The graph revealed that all the samples have almost the same pattern, which is evidence that the crystal structure was consistence for all the doped and undoped thin films [52]. However, a variation was observed in the intensity of the peaks as well as in the sharpness, which is believed to have resulted from the differences in grain size, preferred orientation, crystallinity, strain, or defects. Mirror shift and prominent intensity peaks appeared in samples 5ml (Er, Sr): MnS, 10ml (Er, Sr): MnS, and 15ml (Er, Sr): MnS, showing grain size increment, MnS substitution by Er and Sr or lattice distortion and improvement in the crystallinity as a result of dopants effect. Based on our observation, the notable peaks found when 2theta angles equal 29°, 34.5°, 49.5°, 58.6°, and 68.3° are proportional to the crystal planes (111), (220), (200), (311), and (222), respectively. A clear comparison of the crystal planes found in our study with those of pure MnS shows that our samples retained the cubic α-MnS structures after doping [53]. The results we obtained on the crystal planes of our samples are in agreement with the findings published in the literature [54], about Cr doped ZnS, which retained the original planes of ZnS after doping.

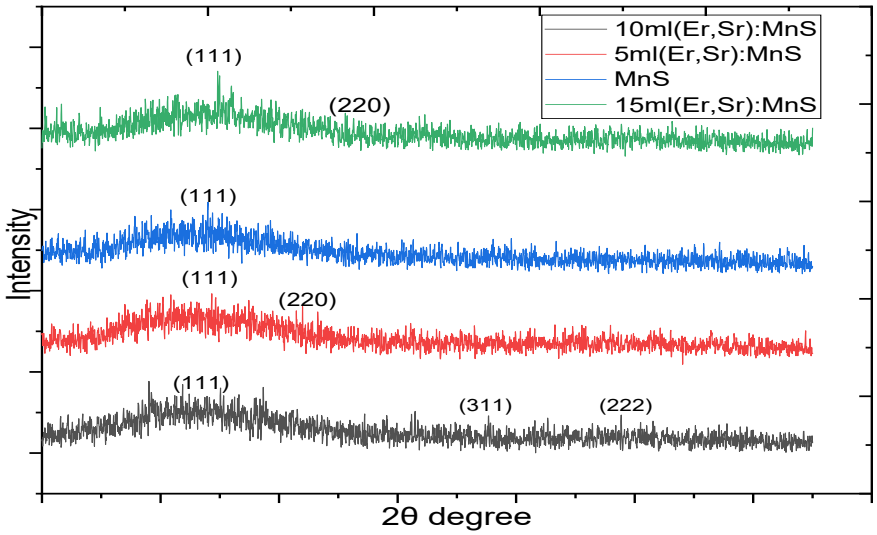

Figure12: XRD of the thin films

4.0 Conclusion

Pure Manganese sulfide and Er /Sr doped MnS thin films were successfully synthesized via chemical spray pyrolysis method, from precursor solution containing 0.8451M solution of manganese (II) sulphate $MnSO_4.H_2O$, 0.1M solution of thioacetamide CH_3CSNH_2, 0.85M solution of Strontium hydroxide and 0.95M solution of Erbium (III) chloride hexahydrate $ErCl_3.6H_2O$. After synthesizing these thin films, they were successfully characterized using different techniques. Based on the results obtained, the following conclusions were made:

1. The spray pyrolysis process was effectively used to create pure MnS and Er/Sr doped MnS thin films.
2. In the visible portion of the solar spectrum, the sample that was synthesised using 10 millilitres of Er and Sr exhibits the maximum absorbance.
3. The maximum transmittance across the spectrum occurs in pure manganese sulphide.
4. The thin films' optical bandgap energy varies between 2.33eV and 3.33eV, demonstrating that the bandgap energy decreased as the dopant concentration increased.
5. The presence of Mn, S, Er, and Sr was detected in the EDS analysis while the SEM inages show the presence of the doped materials. This investigation, indicates that the study's aim was accomplished and the dopants were effectively integrated into the MnS matrix.
6. The functional groups that are present are C=O, C–H, N–H, S–O, Mn–S, and O–H, according to the FTIR analysis.
7. The prominent peaks at angles 29°, 34.5°, 49.5°, 58.6°, and 68.3° correspond to the crystal planes (111), (220), (200), (311), and (222), respectively.
8. After doping, the MnS structure remained unaltered because the doped films kept their cubic shape.

References

[1] S. G. Ibrahim, "Physical properties of chemically spray deposited nanocrystalline manganese sulfide (MnS) thin films," *J Mater Sci Mater Electron*, vol. 32, pp. 543–550, 2021, doi: https://doi.org/10.1007/s10854-020-04837-y.

[2] S. H. Chaki, S. M. Chauhan, J. P. Tailor, and M. P. Deshpande, "Synthesis of Manganese Sulfide (MnS) Thin Films by Chemical Bath Deposition and Their Characterization," *J. Mater. Res. Technol.*, vol. 6, no. 2, pp. 123–128, 2017, doi: 10.1016/j.jmrt.2016.05.003.

[3] A. M. Ferretti, S. Mondini, and A. Ponti, "Manganese Sulfide (MnS) Nanocrystals: Synthesis, Properties, and Applications," in *Advances in Colloid Science*, M. M. Rahman and A. M. Asiri, Eds., Rijeka: IntechOpen, 2016, p. Ch. 6. doi: 10.5772/65092.

[4] M. R. I. Chowdhury, J. Podder, and A. B. M. O. Islam, "Synthesis and characterization of manganese sulphide thin films deposited by spray pyrolysis," *Cryst. Res. Technol.*, vol. 46, no. 3, pp. 267–271, 2011, doi: 10.1002/crat.201000549.

[5] J. Zhang, R. Shi, C. Zhang, L. Li, J. Mei, and S. Liu, "Solvothermal synthesis of manganese sulfides and control of their phase and morphology," *J. Mater. Res.*, vol. 33, no. 24, pp. 4224–4232, 2018, doi: 10.1557/jmr.2018.365.

[6] A. M. Alanazi *et al.*, "Structural Investigations of α-MnS Nanocrystals and Thin Films Synthesized from Manganese (II) Xanthates by Hot Injection, Solvent-Less Thermolysis, and Doctor Blade Routes," *ACS Omega*, vol. 6, no. 42, pp. 27716–27725, 2021, doi: 10.1021/acsomega.1c02907.

[7] A. M. Ferretti, S. Mondini, and A. Ponti, "Manganese Sulfide (MnS) Nanocrystals: Synthesis, Properties, and Applications," in *Advances in Colloid Science*, 2017, ch. 6, pp. 1–35. doi: http://dx.doi.org/10.5772/65092.

[8] S. Sharma, J. Kashyap, S. Gupta, and A. Kapoor, "Effect of Aluminum and Yttrium Doping on Zinc Sulphide Nanoparticles," in *International Conference on Condensed Matter and Applied Physics*, American Institute of Physics, 2016, pp. 1–5. doi: 10.1063/1.4946748.

[9] W. Yu, J. Zhang, and T. Peng, "New insight into the enhanced photocatalytic activity of N-, C- and S-doped ZnO photocatalysts," *Appl. Catal. B, Environ.*, pp. 1–32, 2015, doi: 10.1016/j.apcatb.2015.07.031.

[10] S. Adjokatse, S. Kahmann, H. Duim, and M. A. Loi, "Effects of strontium doping on the morphological, structural, and photophysical properties of FASnI 3 perovskite thin films," *APL Mater*, vol. 7, no. 031116, pp. 1–7, 2019, doi: 10.1063/1.5087110.

[11] R. N. Bulakhe, "Synthesis and Characterization of Pb-Doped MnS Thin Films," vol. 1800211, pp. 2–5, 2019, doi: 10.1002/masy.201800211.

[12] N. Kandasamy and S. Saravanan, "Synthesis and Characterization of Mercury doped and un-doped Manganese Synthesis and Characterization of Mercury doped and un-doped Manganese Sulfide Nanostructure," 2022.

[13] M. Mohammad, F. Jamali-sheini, and R. Yousefi, "Microwave-assisted solvothermal synthesis and physical properties of Zn-doped MnS nanoparticles," *Solid State Sci.*, pp. 1–31, 2018, doi: 10.1016/j.solidstatesciences.2018.10.010.

[14] T. Veeramanikandasamy, K. Rajendran, K. Sambath, and P. Rameshbabu, "Effect of Cu-doping on optical, electrical and magnetic properties of chemically synthesized MnS nanocrystals," *Mater. Chem. Phys.*, pp. 6–13, 2016, doi: 10.1016/j.matchemphys.2016.01.024.

[15] A. Admuthe, S. S. Kumbhar, S. K. Chougule, G. N. Padasare, and M. M. Tonape, "Synthesis and Characterization of MnS Thin Film at Room Temperature for Supercapacitor Application," *Macromol. Symp.*, vol. 392, no. 1, pp. 1–6, 2020, doi: 10.1002/masy.202000186.

Received: 10/07/2025; Revised: 21/07/2025; Accepted: 29/07/2025; Published: 15/09/2025

[16] S. H. Chaki, S. M. Chauhan, J. P. Tailor, and M. P. Deshpande, "Synthesis of manganese sulfide (MnS) thin films by chemical bath deposition and their characterization," *J. Mater. Res. Technol.*, vol. 6, no. 2, pp. 123–128, 2017, doi: https://doi.org/10.1016/j.jmrt.2016.05.003.

[17] S. S. Dhasade, R. S. Gaikwad, S. B. Patwari, and S. Patil, "Synthesis of nanoflakes-like shapes of Manganese sulfide grown at room temperature by electrodeposition method," *J. Chinese Adv. Mater. Soc.*, vol. 3682, pp. 1–21, 2016, doi: 10.1080/22243682.2016.1181529.

[18] S. H. Dhawankar and D. B. Zade, "Manganese Sulphide (MnS) thin film by Spray Pyrolysis technique Abstract: Introduction:" *Int. Res. J. Humanit. Interdiscip. Stud.*, vol. 2, no. 6, pp. 25–29, 2021, doi: http://doi-ds.org/doilink/06.2021-39494537/IRJHIS2106005.

[19] X. Yu, C. Li-yun, H. Jian-feng, F. J. Liu Jia, and Y. Chun-yan, "property of γ-MnS thin films prepared by microwave hydrothermal," *J. Alloys Compd.*, vol. 549, pp. 1–5, 2013, doi: https://doi.org/10.1016/j.jallcom.2012.09.032.

[20] K. Alnama, B. Abdallah, and S. Kanaan, "Deposition of ZnS thin film by ultrasonic spray pyrolysis: effect of thickness on the crystallographic and electrical properties," *Compos. Interfaces*, pp. 1–16, 2016, doi: 10.1080/09276440.2017.1236538.

[21] S. A. Fadaam, H. M. Ali, A. H. Shaban, and S. A. Ahmed, "Improving efficiency of solar cell for MnS through annealing," in *AIP Conference Proceedings*, AIP Publishing, 2020.

[22] X. Xu, S. Li, J. Chen, S. Cai, Z. Long, and X. Fang, "Design Principles and Material Engineering of ZnS for Optoelectronic Devices and Catalysis," *Adv. Funct. Mater.*, vol. 1802029, pp. 1–24, 2018, doi: 10.1002/adfm.201802029.

[23] M. A. Ahaneku, O. L. Ifeanyichi, S. A. Victor, and O. O. Peter, "Synthesis of Bi / Sr doped zinc sulphide by spray pyrolysis technique: Effects of doping concentration on optoelectronic properties," *Chem. Data Collect.*, vol. 41, no. 100942, pp. 1–10, 2022, doi: 10.1016/j.cdc.2022.100942.

[24] S. I. Okpara, D. Tatjana, and G. Inga, "Deposition and Properties of ZnS:Mn Thin Films and Nanostructured Layers by Spray Pyrolysis Method," Tallinn University of Technology, 2018.

[25] R. B. Pujaria, G. S. Gundb, S. J. Patila, H. S. Parkb, and D.-W. Lee, "Anion-exchange phase control of manganese sulfide for oxygen evolution reactions," *J. Mater. Chem. A*, pp. 1–29, 2020, doi: 10.1039/C9TA10553K.

[26] S. Dk, J. Sk, S. Rv, K. Rv, and B. Rn, "Preparation of MnS thin films by chemical bath deposition and effect of bath temperature on their optical propertie," no. 63628, pp. 91–94, 2017.

[27] K. Sushama and S. P. Singh, "Synthesis and Characterization of Zinc Sulphide Nanoparticles," in *3rd International Conference on Condensed Matter and Applied Physics*, 2020, pp. 5–8.

[28] A. A. Adam and K. Ramamurthi, "Effects of Solvent on the Structural and Optical Properties of Spray Deposited Zinc Oxide Thin Films," *Int. J. Adv. Chem. Sci. Appl.*, vol. 3, no. 3, pp. 1–6, 2019.

[29] M. M. Bhagat, L. P, and H. A. Mujawar, "Effect of Tin and Strontium Doping on the Photocatalytic Activity of Zinc Sulphide Nanoparticles for the Photocatalytic Degradation of Resorcinol under Solar and Ultra-Violet Light," *J. Nanosci.*, vol. 3, no. 2, pp. 1–7, 2018, doi: 10.4172/2572-0813.1000122.

[30] M. M. Rashad, D. A. Rayan, and K. El-Barawy, "Hydrothermal Synthesis and Magnetic Properties of Mn Doped ZnS Nanoparticles," *J. Phys. Conf. Ser.*, pp. 1–5, 2010, doi: 10.1088/1742-6596/200/7/072077.

[31] R. Sahraei and S. Darafarin, "Preparation of Nanocrystalline Ni Doped ZnS Thin Films by Ammonia-Free Chemical Bath Deposition Method and Optical Properties," *J. Lumin.*, vol. 149, pp. 170–175, 2014, doi: 10.1016/j.jlumin.2014.01.040.

[32] A. Attaf *et al.*, "Physical Properties of Pb Doped ZnS Thin Films Prepared by Ultrasonic Spray Technique," *Phys. Lett. A*, vol. 1, p. 126199, 2019, doi: 10.1016/j.physleta.2019.126199.

[33] P. O. Offor *et al.*, "Chemical Spray Pyrolysis Deposition of Zinc Sulphide Thin Films Using Ethylenediaminetetraacetic Acid Disodium Salt Complexant," *J. Solid State Electrochem.*, vol. 21, no. 9, pp. 2687–2697, 2017, doi: 10.1007/s10008-017-3668-2.

[34] A. M. Al-Diabat, N. M. Ahmed, M. R. Hashim, and K. M. Chahrour, "Influence of the Spray Distance to Substrate on Optical Properties of Chemically Sprayed ZnS Thin Films," *J. Mater. Sci. Mater. Electron.*, pp. 1–5, 2016, doi: 10.1007/s10854-016-5532-z.

[35] J. P. Espinos, F. Martı, D. Leinen, J. R. Ramos-barrado, and M. C. Lo, "Growth of ZnS Thin Films Obtained by Chemical Spray Pyrolysis: The Influence of Precursors," *J. Cryst. Growth*, vol. 285, pp. 66–75, 2005, doi: 10.1016/j.jcrysgro.2005.07.050.

[36] A. A. Ajayi, A. B. Alabi, and O. W. Abodunrin, "Influence of Solvents on Properties of ZnS Thin Films Synthesized by Chemical Spray Pyrolysis Technique," *Jordan J. Phys.*, vol. 14, no. 4, pp. 347–356, 2021.

[37] C. Falcony, M. A. Aguilar-frutis, and M. Garc, "Spray Pyrolysis Technique; High- K Dielectric Films and Luminescent Materials: A Review," *micromachines*, vol. 9, no. 414, pp. 1–33, 2018, doi: 10.3390/mi9080414.

[38] D. Perednis and L. J. Gauckler, "Thin Film Deposition Using Spray Pyrolysis," *J. Electroceramics*, vol. 14, no. 2, pp. 103–111, 2005, doi: 10.1007/s10832-005-0870-x.

Received: 10/07/2025; Revised: 21/07/2025; Accepted: 29/07/2025; Published: 15/09/2025

[39] M. U. Sarki, M. A. Bilya, and N. A. Iro, "Optical Characterization of Zinc Sulfide (ZnS) Thin Films by Aerosol Assisted Chemical Vapour Deposition (AACVD)," in *Material and Nanomayerias M&Ns-19*, 2019, pp. 1–16.

[40] F. S. Rocha, A. J. Gomes, C. N. Lunardi, S. Kaliaguine, and G. S. Patience, "Experimental methods in chemical engineering: Ultraviolet visible spectroscopy—UV-Vis," *Can. J. Chem. Eng.*, vol. 96, no. 12, pp. 2512–2517, 2018.

[41] R. Boulkroune *et al.*, "Hydrothermal synthesis of Strontium-Doped ZnS Nanoparticles : Structural, Electronic and Photocatalytic Investigations," *Bull. Mater. Sci.*, vol. 42, no. 223, pp. 1–8, 2019, doi: 10.1007/s12034-019-1905-2.

[42] M. A. Ahaneku, O. L. Ifeanyichi, S. A. Victor, and O. O. Peter, "Synthesis of Bi / Sr doped zinc sulphide by spray pyrolysis technique: Effects of doping concentration on optoelectronic properties," *Chem. Data Collect.*, vol. 41, no. 100942, pp. 1–10, 2022, doi: 10.1016/j.cdc.2022.100942.

[43] D. Tatar and B. Düzgün, "The Relationship Between the Doping Levels and Some Physical Properties of SnO2: Thin Films Spray-Deposited on Optical Glass," *Pramana - J. Phys*, vol. 79, no. 1, pp. 137–150, 2012.

[44] N. F. Mott and E. Davis, "Electronic Processes in Non-crystalline Materials," Oxford: Clarendon Press, 1971.

[45] S. Siyalo, H. F. Etefa, and F. B. Dejene, "Enhancing Structural and Optical Properties of CuO Thin Films through Gallium Doping: A Pathway to Enhanced Photoluminescence and Predict for Solar Cells Applications," *Chem. Phys. Impact*, vol. 10, p. 100832, 2025.

[46] R. Siburian, H. Sihotang, s. l Raja, M. Supeno, and C. Simanjuntak, "New Route to Synthesize of Graphene Nano Sheets," *Orient. J. Chem.*, vol. 34, no. 1, pp. 182–187, 2018, doi: 10.13005/ojc/340120.

[47] V. Beena *et al.*, "Synthesis and characterization of Sr-doped ZnSe nanoparticles for catalytic and biological activities," *Water*, vol. 13, no. 16, p. 2189, 2021.

[48] M. Rajasekaran, A. Arunachalam, and P. Kumaresan, "Structural, morphological and optical characterization of Ti-doped ZnO nanorod thin film synthesized by spray pyrolysis technique," *Mater. Res. Express*, vol. 7, no. 3, p. 36412, 2020.

[49] M. R. Bodke, Y. Purushotham, and B. N. Dole, "Crystallographic and optical studies on Cr doped ZnS nanocrystals," *Cerâmica*, vol. 60, pp. 425–428, 2014.

[50] J. Liao, S. Cheng, H. Zhou, and B. Long, "Al-doped ZnS thin films for buffer layers of solar cells prepared by chemical bath deposition," *Micro Nano Lett.*, vol. 8, no. 4, pp. 211–214, 2013.

[51] S. Gao, Y. Lu, T. Ma, H. Liu, and J. Zhang, "Preparation and Photocatalytic Hydrogen Production of Pink ZnS," *Inorganics*, vol. 13, no. 5, p. 166, 2025.

[52] S. Biswas, S. Kar, and S. Chaudhuri, "Solvothermal synthesis of α-MnS single crystals," *J. Cryst. Growth*, vol. 284, no. 1–2, pp. 129–135, 2005.

[53] M. Bodke, H. Khawal, U. Gawai, and B. Dole, "Synthesis and characterization of chromium doped zinc sulfide nanoparticles," *Open Access Libr. J.*, vol. 2, no. 5, pp. 1–8, 2015

Received: 10/07/2025; Revised: 21/07/2025; Accepted: 29/07/2025; Published: 15/09/2025